NJC

Accepted Manuscript

This is an *Accepted Manuscript*, which has been through the Royal Society of Chemistry peer review process and has been accepted for publication.

Accepted Manuscripts are published online shortly after acceptance, before technical editing, formatting and proof reading. Using this free service, authors can make their results available to the community, in citable form, before we publish the edited article. We will replace this *Accepted Manuscript* with the edited and formatted *Advance Article* as soon as it is available.

You can find more information about *Accepted Manuscripts* in the Information for Authors.

Please note that technical editing may introduce minor changes to the text and/or graphics, which may alter content. The journal's standard Terms & Conditions and the Ethical guidelines still apply. In no event shall the Royal Society of Chemistry be held responsible for any errors or omissions in this *Accepted Manuscript* or any consequences arising from the use of any information it contains.

ROYAL SOCIETY OF CHEMISTRY

www.rsc.org/njc

Catalysis of the hydro-dechlorination of 4-chlorophenol and the reduction of 4-nitrophenol by Pd/Fe_3O_4@SiO_2@m-SiO_2

*Yansheng Liu, Wei Zhang, Xinlin Li, Xuanduong Le and Jiantai Ma**

Gansu Provincial Engineering Laboratory for Chemical Catalysis, College of Chemistry and Chemical Engineering, Lanzhou University, Lanzhou 730000, PR China.

** Corresponding author, E-mail addresses: majiantai@lzu.edu.cn (Jiantai Ma).*

Tel.: +86 0931 891 2577; Fax: +86 0931 891 2582

Abstract

In this study, Pd nanoparticles functionalized on the surface of Fe_3O_4@SiO_2@m-SiO_2 nano-catalyst has been synthesised with accessible active sites and ultra-large surface areas. Pd/Fe_3O_4@SiO_2@m-SiO_2 nano-catalyst can be recovered by applying an external magnetic field. The catalyst activity of Pd/Fe_3O_4@SiO_2@m-SiO_2 is tested in the catalytic reduction of 4-nitrophenol and the hydrodechlorination of 4-chlorophenol. The high catalytic activity owes to well-dispersed Pd nanoparticles on the ultra-large surface of Fe_3O_4@SiO_2@m-SiO_2. Furthermore, the Pd/Fe_3O_4@SiO_2@m-SiO_2 nano-catalyst can be reused for at least five times without significant loss in activity, which confirms its good stability. Therefore, the approach mentioned above that based on core-shell structured magnetic Pd/Fe_3O_4@SiO_2@m-SiO_2 provides a useful platform for the fabrication of Pd NPs based catalysts that feature easy accessibility, superior activity and convenient recovery.

1. Introduction

Nowadays, the environmental pollution caused by organic wasters has become an un-ignorable issue.[1] 4-chlorophenol (4-CP) and 4-nitrophenol (4-NP) as important industrial raw materials have been widely applied in important industrial processes, such as the production of germicides, algaecides, fungicides, herbicides, dyes, wood protectors, explosives and plant growth regulators.[2, 3] In the application of 4-CP and 4-NP, a lot of environmental pollutions have been produced. Among the most harmful organic contaminants, 4-CP is considered as a hazardous pollutant because of its acute toxicity and strong bioaccumulation potential[4]. And 4-NP is also regarded as a notorious industrial pollutant and environmentally hazardous material because of its high solubility and stability in water.[5, 6] So how to deal with these kinds of pollution has become increasingly important and no time to delay. Up to now, there are many methods including thermal have been reported to dispose the wastewater that contains 4-CP or 4-NP. They are combustion, reduction dechlorination,[7, 8] oxidation dechlorination,[9] biodegradation, photocatalytic degradation, adsorption[10] and nitro group reduction.[11] The research about how to remove these compounds through an economic and environmentally friendly way has attracted many researchers' attention. After weighting pros and cons, the reduction of nitro group to amidogen is commonly used for 4-NP, and the hydrodechlorination process is used for the degradation of 4-CP as an economic, environmental and efficient way. Moreover, the reduction

product 4-aminophenol (4-AP) is an extremely useful organic compound that has been employed in various applications[12] and the only product (phenol) can be subsequently recycled.[13, 14]

The liquid phase catalytic HDC of 4-CP has been studied by many groups.[15-17] The studies in the literature mainly focus on the catalytic activities which are affected by active phase, support, sources of hydrogen, or reaction media.[18, 19] By summarizing the experience of pioneers, the HDC treatment of CPs uses noble metals as activity phase and molecular hydrogens as hydrogen source, which is an efficient method.[20] Till now, large numbers of catalysts using metal nanoparticles (NPs) (such as Pd[19, 21-24], Pt[25, 26], Rh[27], Ni[15]) and some supported bimetallic catalysts (such as: Pd-Bi,[28, 29], Pd–Tl[30], Pd-Fe[31], and Ni@Pd[32]) as active phases have been extensively researched. Among them, Pd based catalysts show an excellent catalytic activity for the treatment of 4-CP at room temperature and atmospheric pressure.

According to the studies of J. A. Baeza [33] and M. A. Aramendia[34], it seems that HDC is a structure-sensitive reaction. The effects of supports in HDC reactions have been extensively studied. Recently, researches have demonstrated that the choice of support has a significant influence on the dispersion and electronic properties of the NPs. Many supports, such as activated carbon (AC),[35-37] Al_2O_3[38] or zeolites[39, 40] have been employed to prepare catalysts for the HDC of 4-CP. The studies show that Al_2O_3 as support can improve the stability of active species of the catalyst. Nevertheless, this metal oxide support is more sensitive to HCl produced during the HDC process.

Compared with Al_2O_3, AC seems more suitable as support because of its high surface area and particular physical and chemical properties. However, the strong adsorption properties based on surface area, pore size distribution, and surface composition all limit the applications of AC. So large numbers of SiO_2 based support has been synthesised and applied in the catalytic reactions, such as mesoporous SiO_2, SBA-15, MCM-41, MCM-48 and so on. These supports possess unique pore structure and large surface areas which can affect the catalytic activity of activity phase. In addition, in order to make the nanocatalyst to be separated and recovered from the reaction mixture easily, there are lots of magnetic nanocatalysts have been synthesised, such as Fe_3O_4@m-SiO_2,[41, 42] Fe_3O_4@SiO_2@KCC-1,[43] Fe_3O_4@C,[44, 45] Fe_3O_4@MCM-41[46] and so on.

In our previous work, several SiO_2 based catalysts have been applied in the HDC of 4-CP, such as Pd/MCM-48 nanosphere,[47] Pd/dendritic mesoporous silica nanospheres[48] and Pd/KCC-1[49]. Compared with the catalysts mentioned above, Fe_3O_4@SiO_2@m-SiO_2 exhibits higher catalytic activity.

In this study, active phase focuses on Pd NPs, because of their excellent catalytic activity in the HDC of 4-CP and the reduction of 4-NP. Considering that the catalytic activity can be affected by surface area and the character of easy recovery, Fe3O4@SiO2@m-SiO_2 has been used as a support, which makes Pd NPs well dispersed and the reactant molecule more easily connected with activity phases.

Besides, by using a magnet, the Pd/Fe_3O_4@SiO_2@m-SiO_2 nanocatalyst can be quickly, easily and thoroughly separated from the reaction system.

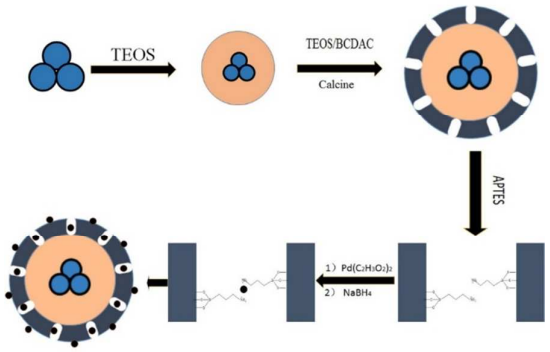

Scheme 1. Preparation of Pd/Fe_3O_4@SiO_2@m-SiO_2 nanocatalyst

2. Experimental

2.1 Materials

Tetraethoxysilane (TOES), Pd(II) acetate, (3-aminopropyl) triethoxysilane (APTES) Hexadecyl trimethyl ammonium Bromide (CTAB) and Benzylcetyldimethylammonium chloride (BCDAC) are purchased from Aladdin Chemical Co., Ltd. 4-Chlorphenol (4-CP), 2-Chlorphenol (2-CP) , 2,4-Dichlorophenol (2,4-DCP), 4-nitrophenol (4-NP) and concentrated ammonia aqueous solution are purchased from Lanzhou Aihua Chemical Company. $NaBH_4$ is supplied by Sinophrm Chemical Reagent Co., Ltd. Oganic solvents are of analytical grade and do not require further purification.

2.2 Preparation of Fe_3O_4@SiO_2@m-SiO_2 nanoshpere

The Fe_3O_4@SiO_2 spherical magnetic particles are fabricated according to a literature procedure.[50] Then, the Fe_3O_4@SiO_2@m-SiO_2 sphere is synthesized as follows: Fe_3O4@SiO_2 NPs (250 mg) are dispersed in mixed solution with 330 mg of

BDCAC and 145 mL of distilled water under ultrasonication for 30 min. Then, 1.5 mL of TEOS is added to the solution drop-wise under mechanical stirring for 2 h and then aged at 90 °C for 48 h. The product is centrifuged, washed repeatedly with ethanol and distilled water, and then dried in vacuum at 40 °C overnight. The dry product is calcined at 600 °C for 3 h at a rate of temperature increasing 5 °C min^{-1}.

2.3 Preparation of Pd/Fe_3O_4@SiO_2@m-SiO_2 nanoshpere

Firstly, Fe_3O_4@SiO_2@m-SiO_2 nanoshpere is functionalized with APTES to obtain Fe_3O_4@SiO_2@m-SiO_2-NH_2 nano-composites. Secondly, 500 mg of Fe_3O_4@SiO_2@m-SiO_2-NH_2 nanocomposite is added into a 100 mL round-bottom flask with 54 mg of $Pd(OAc)_2$ and 50 mL of acetonitrile, then ultrasonically dispersed for 30 min and keep stirring for 12 h. Subsequently, the fresh $NaBH_4$ solution (0.2 M, 20 mL) is added drop-wise into the above suspension. The catalyst is collected by filtration, washed several times with ethanol, and dried overnight under vacuum at 40 °C.

2.4 General procedure for the hydrodechlorination of CPs

HDC experiments are performed in a three-necked jacketed glass reactor at H_2 atmosphere. 10 mg of catalyst is placed into the mixed solution of 40 mL solvent, 0.5 mmol of reactant and 0.5 mmol of base under vigorous stirring at 30℃– 35℃. The results of the experiments are analysed by gas chromatograph-mass spectrometer (GC-MS).

2.5 General procedures for the reduction of 4-NP

The reduction of 4-NP by $NaBH_4$ is chosen as a model reaction for investigating the catalytic performance of $Pd/Fe_3O_4@SiO_2@m\text{-}SiO_2$ nanocatalyst. In short, 3.0 mL of deionized water and 30 μL of 4-NP (0.01 M) are mixed with 0.5 mL of freshly prepared aqueous $NaBH_4$ solution (0.5 M), resulting in the formation of a deep yellow solution. Then, 2 μL of $Pd/Fe_3O_4@SiO_2@m\text{-}SiO_2$ nanocatalyst (2 mg mL^{-1}) is added to this resulting solution, and the reaction is allowed to proceed until the solution became colorless. The reaction conversion is determined by the ultraviolet visible spectroscopy (UV-Vis)

2.6 General methods

Powder X-ray diffraction (XRD) spectra are obtained by using a Rigaku D/max-2400 diffractometer and using Cu-Kα radiation in the 2θ range of 10–90°. Fourier transform infrared (FT-IR) spectra are collected on a Nicolet Nexus 670 FT-IR spectrometer that equipped with a deuterated triglycine sulfate pyroelectric detector by using KBr pellets. Transmission electron microscopy (TEM) images are obtained on a Tecnai G2 F30, FEI, USA. The UV-Vis measurement is conducted with the UV2800PC UV-Vis spectrophotometer. Magnetic measurements of $Fe_3O_4@SiO_2@m\text{-}SiO_2$ and $Pd/Fe_3O_4@SiO_2@m\text{-}SiO_2$ are performed by using a quantum design vibrating sample magnetometer (VSM) at room temperature in an applied magnetic field sweeping from −15 to 15 KOe. The reaction conversion is estimated by using GC (P.E. Auto System XL) or GC–MS (Shimadzu QP2010S).

3. Results and Discussion

In the synthesis of mesoporous silica materials, CTAB[51-53], CTAC[54] are always used as templates. Compared with CTAB, BCDAC has a nearly identical tail length and volume, but the additional π–π interactions between the benzyl groups of the adjacent molecules would slightly compensate for the repulsion between the quaternary ammonium head groups, rendering the surfactant with a smaller effective head group area.[55, 56] Compared with the mesoporous SiO_2 that uses CTAB as the template, BCDAC brings uniform sizes and morphology, and the large surface of mesoporous SiO_2. For example, in the studies of Yonghui Deng[42] and Wenru Zhao,[57] the BET surface areas of mesoporous SiO_2 materialare 365 $m^2 g^{-1}$ and 283 $m^2 g^{-1}$, respectively. In our study, the BET surface area of catalyst is 955.8 $m^2 g^{-1}$, which is higher than that of the reported mesoporous SiO_2 materials.

3.1 Characterization

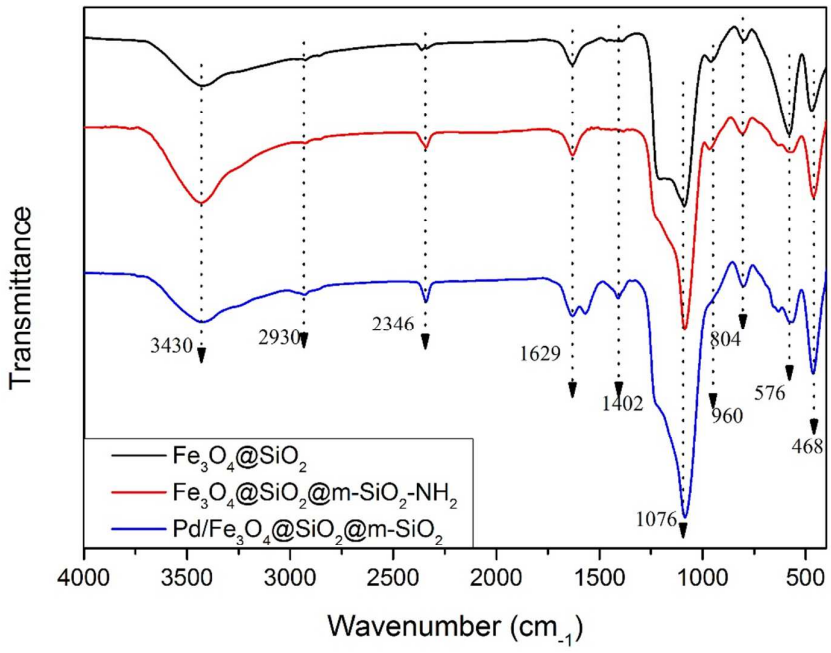

Figure1. FT-IR spectra of Fe_3O_4@SiO_2, Fe_3O_4@SiO_2@m-SiO_2-NH_2 and Pd/Fe_3O_4@SiO_2@m-SiO_2.

Figure 1 shows the FT-IR spectra of the Fe_3O_4@SiO_2, Fe_3O_4@SiO_2@m-SiO_2-NH_2 and Pd/Fe_3O_4@SiO_2@m-SiO_2. In the two samples, the typical Si–O–Si bands around 1100 cm^{-1} and 800 cm^{-1} associate with the formation of a condensed silica network. FTIR bands observed at 960, 468, and 576 cm^{-1} correspond to Si-OH, Si-O, and Fe-O stretching, respectively. The strong FTIR band at 3430 cm^{-1} shows large amount of Si–OH groups which are proved to be advantageous for the modification of APTES on the SiO_2 surface by hydrogen bonds. The band at 2930 cm^{-1} corresponds to -CH stretching. In the FT-IR spectrum of Fe_3O_4@SiO_2, Fe_3O_4@SiO_2@m-SiO_2-NH_2 and Pd/Fe_3O_4@SiO_2@m-SiO_2, the bands around 3430 cm^{-1} represent the adsorption of –OH and –NH_2 groups. The proportion of nitrogen, hydrogen, and carbon in Fe_3O_4@SiO_2@m-SiO_2 are 0.0%, 1.03%, and 0.398%; and the proportion of nitrogen, hydrogen, and carbon in Pd/Fe_3O_4@SiO_2@m-SiO_2 are 1.23%, 5.76%, and 0.868% respectivly, which are measured by the elementary analysis. The FT-IR spectra and the elementary analysis result reveal that the APTES is successfully grafted on the Fe_3O_4@SiO_2@m-SiO_2 surface, thus enabling them to act as robust anchors for metal NPs.

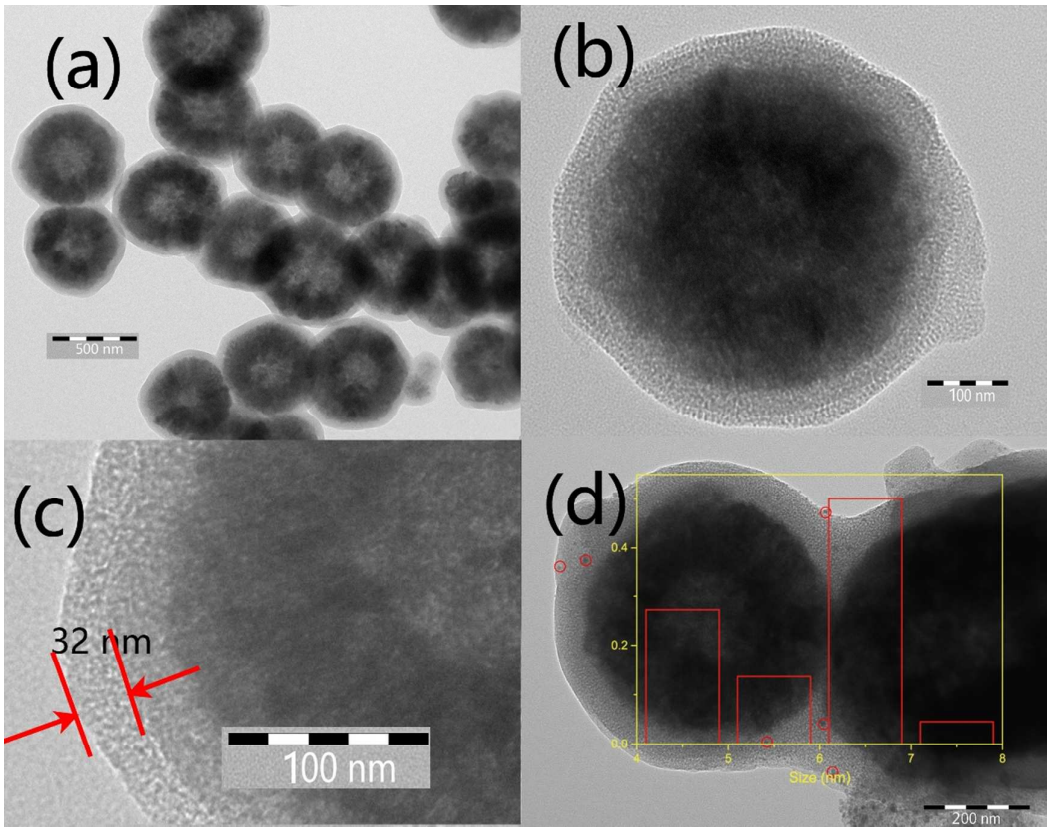

Figure 2. TEM image of Fe_3O_4@SiO_2(a), Fe_3O_4@SiO_2@m-SiO_2 (b), Pd/Fe_3O_4@SiO_2@m-SiO_2 (d) and partial enlarged drawing (c) of Fe_3O_4@SiO_2@m-SiO_2

The synthesis procedure of Pd/Fe_3O_4@SiO_2@m-SiO_2 nanaocatalyst is represented in Scheme 1 and described in detail in the experimental section. TEM and SEM images of Pd/Fe_3O_4@SiO_2@m-SiO_2 with 4.75% metal loading which are calculated by the inductive coupled measurement are shown in Figure 1. Figure 1b shows a typical TEM image of prepared Fe_3O_4@SiO_2@m-SiO_2 core-shell structured NPs. From Figure 1a and Figure 1d, it can be observed that mesoporous SiO_2 is capped on the surface of Fe_3O_4@SiO_2 core. It can also be measured that average diameter of Fe_3O_4@SiO_2 core is about 400 nm and the thicknesses of mesoporous SiO_2 shell is about 32 nm. According to the TEM image (Figure 2d) of

Pd/Fe_3O_4@SiO_2@m-SiO_2, size frequency curve is obtained (inset of Figure 2d). Also,size distribution of Pd NPs has been made, and the main size of Pd NPs range is between 4-7 nm.

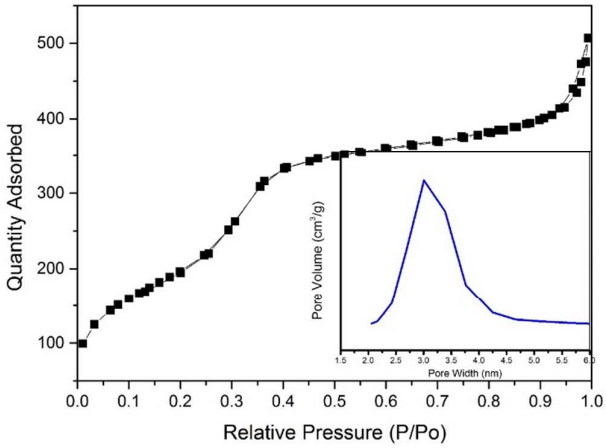

Figure 3. Nitrogen adsorption–desorption isotherms and pore size distribution (*inset*) of Pd/Fe_3O_4@SiO_2@m-SiO_2

N_2 adsorption-desorption isotherms for the Pd/Fe_3O_4@SiO_2@m-SiO_2 are given in Figure 3. According to the IUPAC classification, the curves of as-prepared sample are typical IV isotherms with a very sharp capillary condensation step at P/P_0 = 0.3–0.5 and H_4-type hysteresis loop, characterizing small-pore mesoporous materials. The pore size of as-prepared catalyst derived from the BJH analysis on the desorption branch is 3.0 nm. The calculated BET surface area and pore volume of Pd/Fe_3O_4@SiO_2@m-SiO_2 are 955.8 m^2 g^{-1} and 0.78 cm^3 g^{-1}, respectively. And the surface area is much larger than that of the magnetic nanocatalyst, in which Fe_3O_4 is used as a magnetic core. The ultra-large surface area can provide more external surface to load more metal NPs. The channel structure can also provide internal surface area and active sites. Besides, the ultra-large surface area can make the loaded

metal NPs well-distributed. The well-dispersed metal NPs on support enable reactant molecules to combine to active sites more easily and enable product molecules to desorb from active sites more quickly, so that the reaction rate can be raised. These particular characters cannot be found in some other catalysts with small surface areas and non-channel structures.

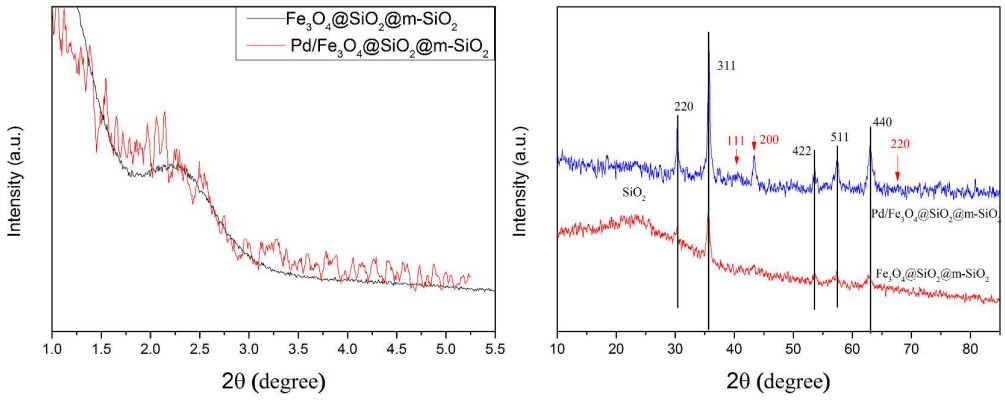

Figure 4. Small-angle (a) and Wide-angle (b) XRD patterns of Fe_3O_4@SiO_2@m-SiO_2 and Pd/Fe_3O_4@SiO_2@m-SiO_2

The small-angle and wide-angle XRD patterns of nanaocatalyst are obtained in Figure 4. There is an intense characteristic peak at 2θ = 2.3°. By comparing the small-angle XRD patterns, it can be observed that the surve belonging to Pd modified Fe_3O_4@SiO_2@m-SiO_2 is not slippy, but it also shows the same tendency with un-modified Fe_3O_4@SiO_2@m-SiO_2. This difference rightly indicates that the Pd NPs has been loadded on the the support and it changes the original structure of support in some sense. From the wide-angle XRD patterns (Figure 4b), it can been seen that Pd/Fe_3O_4@SiO_2@m-SiO_2 possesses three peaks that corresponds to planes (111),

(200), (220) of Pd and the peaks of Fe_3O_4 that corresponds to planes (220) (311) (422) (511) .

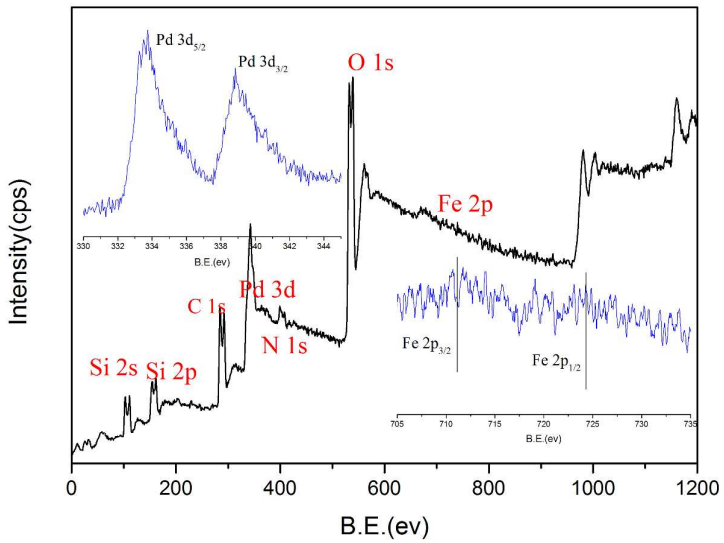

Figure 5. XPS spectra of $Pd/Fe_3O_4@SiO_2@m\text{-}SiO_2$ (*inset: high resolution spectrum of Pd 3d*)

The electronic state of the Pd species on the $Pd/Fe_3O_4@SiO_2@m\text{-}SiO_2$ is measured with XPS. The pattern of $Pd/Fe_3O_4@SiO_2@m\text{-}SiO_2$ catalyst is exhibited in Figure 5. The Pd_{3d} peaks in XPS spectra show that the binding energy values are at 333.7 eV and 339.0 eV, which are attributed to the $3d_{5/2}$ and $3d_{3/2}$ peaks of Pd; and the peaks observed in the XPS spectra of Fe 2p at binding energies of 710.7 and 724.3 ev are characteristic of Fe_3O_4. Because the Fe_3O_4 core is wrapped by SiO_2 and m-SiO_2, so the intensity of XPS peak of Fe is very weak. In addition, the nitrogen has been observed, which also shows the evidence that the TPTES is successfully modified on the $Fe_3O_4@SiO_2@m\text{-}SiO_2$ surface.

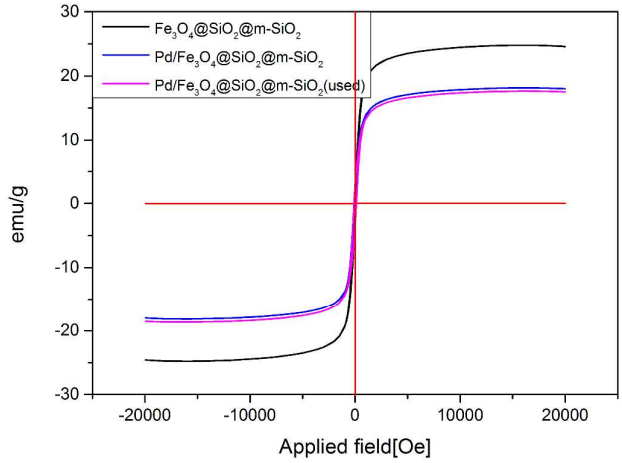

Figure 6. Room temperature magnetization curves of Fe_3O_4@SiO_2@m-SiO_2 and Pd/Fe_3O_4@SiO_2@m-SiO_2 nanocatalyst

Magnetic measurements are carried out by VSM at room temperature. The magnetization curves measured for Fe_3O_4@SiO_2@m-SiO_2 and Pd/Fe_3O_4@SiO_2@m-SiO_2 are shown in Figure 6. The magnetic saturation values of the Fe_3O_4@SiO_2@m-SiO_2, Pd/Fe_3O_4@SiO_2@m-SiO_2 and the used Pd/Fe_3O_4@SiO_2@m-SiO_2 are 24.7, 17.9 and 17.4 emug g^{-1}, respectively. The decrease in the saturation magnetization is due to the presence of the APTES and Pd NPs on the Fe_3O_4@SiO_2@m-SiO_2 surface. Moreover, Figure 6 (inset image) shows the separation-redispersion process of the Pd/Fe_3O_4@SiO_2@m-SiO_2 nanocatalyst, which demonstrates that the catalyst is drawn from the solution to the sidewall of the vial by employing an external magnetic field which has been removed. Therefore, the mentioned results indicate an easy and efficient way to separate and recycle the Pd/Fe_3O_4@SiO_2@m-SiO_2 nanocatalyst from the solution by external magnetic field.

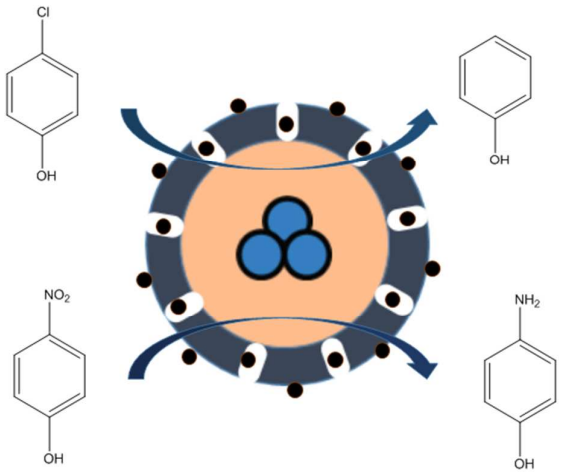

Scheme 2. Reductions of 4-NP and HDC of 4-CP are catalyzed by Pd/Fe_3O_4@SiO_2@m-SiO_2 nanocatalyst respectively

3.2 Catalytic reduction of 4-NP

The catalytic activity of the Pd/Fe_3O_4@SiO_2@m-SiO_2 nanocatalyst is studied by the reduction reaction of 4-NP to 4-AP in the presence of $NaBH_4$. The evolution process with reaction time for the reduction of 4-NP to 4-AP is monitored by UV–VIS spectroscopy. Solution of 4-NP exhibits a strong absorption peak at 317 nm, which is remarkably red-shifted to 400 nm when treated with an aqueous solution of $NaBH_4$, due to the formation of 4-nitrophenolate ions. From Figure 7a, it can be observed that with the time running, the absorption peak intensity of 4-NP is reducing and the absorption peak intensity of 4-NA is increasing. Figure 6b shows the $\ln(C/C_0)$ versus reaction time for the reduction of 4-NP, where C and C_0 are the concentrations of the 4-NP at intervals and the initial stage, respectively. Because that the concentration of $NaBH_4$ is much higher than that of 4-NP, the reduction reactions are assumed to be pseudo first-order, with respect to the con-centration of 4-NP.[58, 59] Thus, pseudo-first-order kinetics could be applied to evaluate the kinetic rate constant (k) of

the current reaction, where A_0 and A_t are absorbance values of 4-NP initially and at time t, respectively.

$$\frac{dC_t}{dt} = -kt \ or \ \ln\frac{C}{C_0} = \ln\frac{A_t}{A_0} = -kt \qquad (1)$$

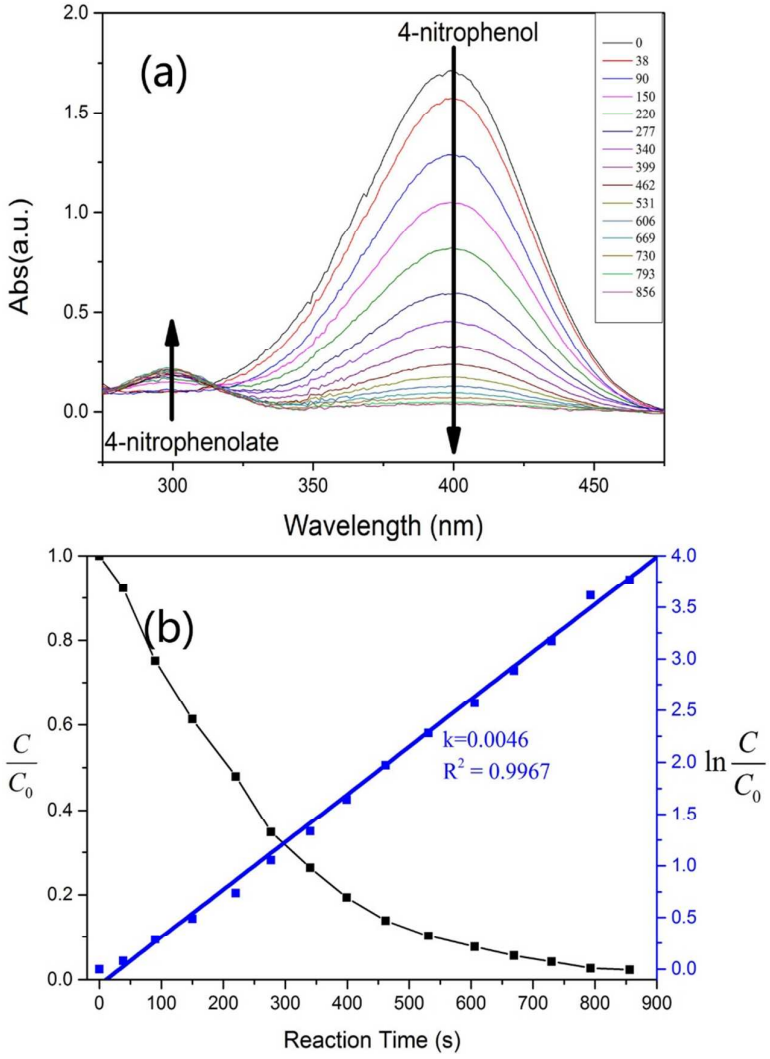

Figure. 7. UV–vis spectra of the successive reduction of 4-NP to 4-AP over the prepared $Pd/Fe_3O_4@SiO_2@m\text{-}SiO_2$ nanocatalyst (a) and plots of Ct/C_0 and $\ln(C/C_0)$ versus reaction time for the reduction of 4-NP over $Pd/Fe_3O_4@SiO_2@m\text{-}SiO_2$ nanocatalyst (b).

The apparent kinetic rate constant (k_{app}) is calculated to be 0.0046 s^{-1} for the reaction catalyzed by using $Pd/Fe_3O_4@SiO_2@m\text{-}SiO_2$ nanocatalyst. Thus, for a quantitative comparison, the normalized rate constant $k_{nor}= k_{app}/C_{Pd}$ is introduced,

which is defined as the ratio of the rate constant k to the molarity of the active sites of Pd added. The reaction rate constant per molarity (C_{Pd}) is calculated to be k_{nor}= 5.3 s^{-1} mM^{-1} by creating the above condition. As for the reduction of 4-NP, it uses Pd/Fe_3O_4@SiO_2@m-SiO_2 nanocatalyst. This values responding to Pd/SBA-15, Pd/PEDOT, Pd/Al_2O_3 Pd/Fe_3O_4@SiO_2@KCC-1 and Ni@Pd/KCC-1 are 0.118 s^{-1} mM^{-1}, 0.261 s^{-1} mM^{-1}, 1.085 s^{-1} mM^{-1}, 2.78 s^{-1} mM^{-1} and 0.163 s^{-1} mM^{-1}, respectively. The excellent catalytic activity of the Pd/Fe_3O_4@SiO_2@m-SiO_2 nanocatalyst owes to the easy access of its active sites, and the well dispersion of the Pd NPs on the Fe_3O_4@SiO_2@m-SiO_2 support. In this situation, reactant can be easily adsorbed on the Pd NPs surface, which allows the reduction reactions to start quickly and finish rapidly.

3.3 HDC of 4-CP

The catalytic activity of nanocatalyst is established by the HDC of CPs under green conditions, and the reaction conditions are established at room temperature and atmospheric pressure and a stirring speed of 1000 rpm. The HDC of 4-CP is negligible without catalyst or in the presence of pure Pd/Fe_3O_4@SiO_2@m-SiO_2 at the same conditions, which shows that the presence of metal NPs is indispensable for high catalytic activity. In some studies, phenol and further hydrogenation product cyclohexanone (CYC) are detected.[25,34] Compared with the reactant 4-CP, the two products detected are of low toxicity and are used as intermediates in the production of high value-added chemicals. In this work, phenol, a high selectivity product, is

observed. So it can be concluded that the further hydrogenation product cyclohexanone could be generated under the condition of high pressure of H_2 and large ratio of Pd/4-CP[60, 61]. In the study of Elena Dı´az[60], 2.5 mg of Pd catalyze 0.05-0.4 mg of CPs per minute. This means 1 mg of CPs is catalysed by 50-6.25 mg of CPs, and this large amount of Pd/initial amount of CPs may be the reason why hydrogenation product cyclohexanone is generated. Compared with reports mentioned above, in our reaction, a batch of stirred tank reactors are used at H_2 atmosphere. The main production is phenol and less than 0.2% of CYC is detected after 100 min of reaction time. These differences may be caused by the use of different reaction systems. This result agrees with the study that uses the same reaction system, in which phenol is detected as a major product.[20, 32, 43, 49, 62]

The HDC reaction pathway is described as below: H_2 adsorbed on the active site of the nanocatalyst is activated into two hydrogen atoms which combined with 4-CP and also adsorbed on the surface of the activity phase. The C-Cl bond of 4-CP is attacked by the active hydrogen atoms to form phenol.[32] The results of exploring optimal reaction condition and the results of HDC of 2-CP, 3-CP, 4-CP and 2,4-DCP by using Pd/Fe_3O_4@SiO_2@m-SiO_2 as catalyst are exhibited in Table 1. In order to reduce HCl inhibition in the process of HDC of 4-CP, four kinds of bases have been studied. By comparing the HDC results, it can be easily summarized that NaOH is the best choice as the base to neutralize HCl.[32] With the addition of base, catalyst deactivation is largely governed by HCl solubility/transport and the nature of the basic

species in the catalyst matrix has been reported with higher HDC rates and enhanced catalyst stability.[63] In addition, organic and inorganic solvents are also detected and compared the HDC result (Table 1), water as solvent in HDC experiments performs well. In the reaction process, NaCl is generated by the neutralization of HCl and NaOH. In organic solvent, low solubility of NaCl can deposit on the surface of catalyst which blocks the pores of support, thereby inhibiting adsorption and activation that result in a decrease of reaction rate.[34] The Figure 8 shows the time-dependent concentration of 4-CP and the concentration of the product phenol in the HDC reaction by using $Pd/Fe_3O_4@SiO_2@m\text{-}SiO_2$ nanocatalyst under the optimum condition.

The results of HDC of 2-CP, 3-CP, 4-CP and 2,4-DCP by using $Pd/Fe_3O_4@SiO_2@m\text{-}SiO_2$ as catalyst are carried out and exhibited in Table 1.

Table 1. The yield of HDC of CPs catalyzed by $Pd/Fe_3O_4@SiO_2@m\text{-}SiO_2$

reactant	Base	Solvent	Yield%
[a]4-CP	Na_2CO_3	H_2O	79.8%
[a]4-CP	NaAc	H_2O	65.4%
[a]4-CP	triethyl amine	H_2O	55.3%
[a]4-CP	NaOH	ethyl acetate	7.8%
[a]4-CP	NaOH	ethyl alcohol	2.5%
[a]4-CP	NaOH	H_2O	100%
[a]2-CP	NaOH	H_2O	100%
[a]3-CP	NaOH	H_2O	100%
[b]2,4-DCP	NaOH	H_2O	55.2%

Reaction conditions: solvent (40 mL), CPs (0.5 mmol), catalyst dosage 20 mg; [a] 1 mmol base, [b] 1 mmol base; reaction time: 100 min

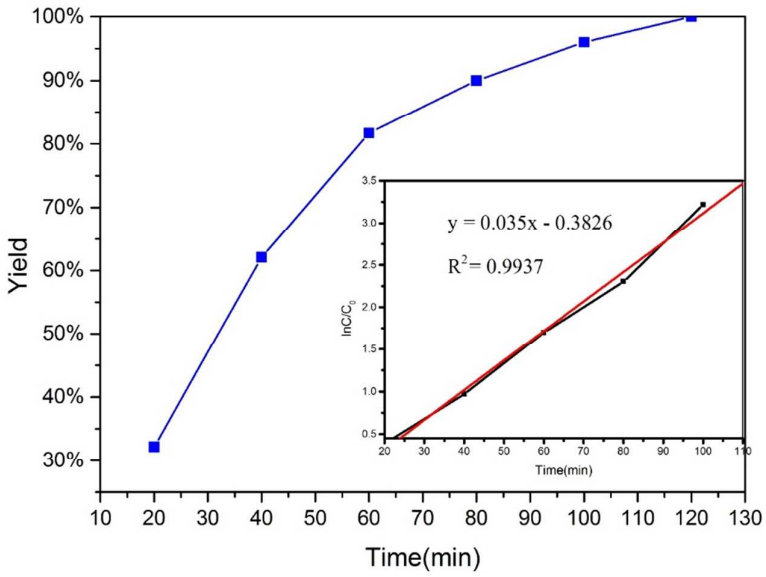

Figure 8. Fitted kinetic rate constants of HDC 4-CP to phenol under the optimum condition

The concentration of H_2 can be considered constant since all the reactions are carried out with a high excess of reactant. Therefore, the reaction follows pseudo-first-order reaction kinetics:

$$R_{4\text{-CP}} = \frac{dC_{4-CP}}{dt} = -r_1 = -k_1 C_{4-CP} \qquad (2)$$

According to the concentration value related to reaction time, through plotting the logarithm of 4-CP concentration versus reaction time, the linear fittings are drawn in Figure 8. The first order kinetic reaction rate constant has been calculated, which is 0.035 min^{-1}. The reaction rate constant per unit mass $k' = k/M_{Pd}$ is calculated to be 37.2 min^{-1} g^{-1}. The kinetic reaction rate of HDC catalysed by Pd/Al_2O_3, Pd/pillared clays catalyst, Pd/DMSN, Pd/KCC nanocatalyst and and Ni@Pd/KCC-1 are 3.33 min^{-1} g^{-1}, 7.6 min^{-1} g^{-1}, 13.2 min^{-1} g^{-1}, 21.15 min^{-1} g^{-1} and 38.1 min^{-1} g^{-1},

respectively.[25, 48, 61, 62] This indicates the good catalytic activity of $Pd/Fe_3O_4@SiO_2@m\text{-}SiO_2$ nanocatalyst.

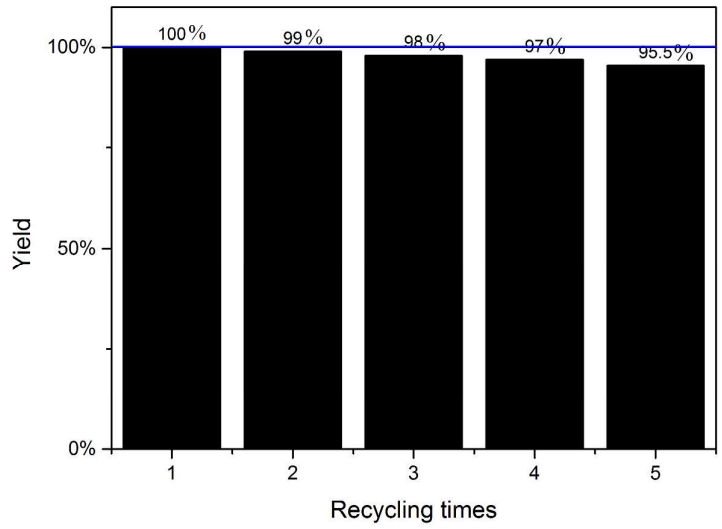

Figure 9. HDC turnover rates of 4-CP HDC over recycled catalyst.

The stability experiment is performed in a flask at H_2 atmosphere. The catalyst is recovered by magnetism and simple decantation of liquid products. The catalyst is then washed with deionized water and used directly for the next cycle of reaction without further purification. The recoverability and reusability are investigated by the HDC reaction of 4-CP and the results are summarized in Figure 9. After 5 times of recycling, the metal loading of catalyst is measured as 4.01% , instead of 4.75 %. And the catalytic activity of $Pd/Fe_3O_4@SiO_2@m\text{-}SiO_2$ reduces very slightly. These results confirm the high rate of the recyclability of the $Pd/Fe_3O_4@SiO_2@m\text{-}SiO_2$.

4. Conclusion

In summary, $Pd/Fe_3O_4@SiO_2@m\text{-}SiO_2$ core–shell structured nanocatalyst has been prepared and the catalytic property is investigated in the reduction of

4-nitrophenol and the hydrodechlorination of 4-chlorophenol as a target compound under the condition of sodium hydroxide aqueous solution and atmospheric H_2 pressure. The magnetism of Fe_3O_4@SiO_2@m-SiO_2 makes the catalyst recycling easier and more convenient. The ultra-large surface area of Fe_3O_4@SiO_2@m-SiO_2 can improve the mass transfer, increase adsorption–desorption rate of compounds and reaction rate, and enable catalyst to possess much more active sites and well-distributed loaded metal particles. By analysing the results of catalytic activity, Pd/Fe_3O_4@SiO_2@m-SiO_2 nanocatalyst shows a good catalytic activity for the hydrodechlorination of 4-chlorophenol with the reaction rate constant per unit mass being $k' = k/M_{Pd}$ is 37.2 min^{-1} g^{-1}, and the reduction of 4-nitrophenol with the reaction rate constant per molarity calculated to be k_{nor}= 5.3 s^{-1} mM^{-1}. The Pd/Fe_3O_4@SiO_2@m-SiO_2 nanocatalyst could be recycled for at least five times in the corresponding reactions without significant deactivation in the catalytic activity. The Pd/Fe_3O_4@SiO_2@m-SiO_2 nanocatalyst act as relatively green, economical, and environmentally friendly catalyst, and as a promising candidate for various Pd based catalytic applications.

References

1. Y. Liu, B. Qiao, X. Li, X. Le, W. Zhang and J. Ma, *J. Mol. Catal. A: Chem.*, 2015, **406**, 65-71.
2. H. J. Amezquita-Garcia, E. Razo-Flores, F. J. Cervantes and J. R. Rangel-Mendez, *Carbon*, 2013, **55**, 276-284.
3. L. Calvo, M. A. Gilarranz, J. A. Casas, A. F. Mohedano and J. Rodriguez, *J. Hazard. Mater.*, 2009, **161**, 842-847.
4. Z. Jin, X. Wang, S. Wang, D. Li and G. Lu, *Catal. Commun.*, 2009, **10**, 2027-2030.
5. J. Feng, L. Su, Y. Ma, C. Ren, Q. Guo and X. Chen, *Chem. Eng. J.*, 2013, **221**, 16-24.
6. M. Zarejousheghani, M. Möder and H. Borsdorf, *Anal. Chim. Acta*, 2013, **798**, 48-55.
7. Y. Han, W. Li, M. Zhang and K. Tao, *Chemosphere*, 2008, **72**, 53-58.
8. W. Zhang, X. Quan, J. Wang, Z. Zhang and S. Chen, *Chemosphere*, 2006, **65**, 58-64.
9. C. E. Hetrick, J. Lichtenberger and M. D. Amiridis, *Appl. Catal. B: Environ.*, 2008, **77**, 255-263.
10. E. Marais and T. Nyokong, *J. Hazard. Mater.*, 2008, **152**, 293-301.
11. L. Zhang, S. Zheng, D. E. Kang, J. Y. Shin, H. Suh and I. Kim, *Rsc Advances*, 2013, **3**, 4692-4703.

12. S. M. El-Sheikh, A. A. Ismail and J. F. Al-Sharab, *New J. Chem.*, 2013, **37**, 2399-2407.

13. J. Zhou, Y. Han, W. Wang, Z. Xu, H. Wan, D. Yin, S. Zheng and D. Zhu, *Appl. Catal. B: Environ.*, 2013, **134–135**, 222-230.

14. S. Gómez‐Quero, F. Cárdenas‐Lizana and M. A. Keane, *AlChE J.*, 2010, **56**, 756-767.

15. E. Diaz, A. F. Mohedano, J. A. Casas, L. Calvo, M. A. Gilarranz and J. J. Rodriguez, *Appl. Catal. B: Environ.*, 2011, **106**, 469-475.

16. M. A. Keane, G. Pina and G. Tavoularis, *Appl. Catal. B: Environ.*, 2004, **48**, 275-286.

17. S. Ordonez, E. Diaz, R. F. Bueres, E. Asedegbega-Nieto and H. Sastre, *J. Catal.*, 2010, **272**, 158-168.

18. H. M. Roy, C. M. Wai, T. Yuan, J. K. Kim and W. D. Marshall, *Appl. Catal. A: Gen.*, 2004, **271**, 137-143.

19. F. D. Kopinke, K. Mackenzie, R. Koehler and A. Georgi, *Appl. Catal. A: Gen.*, 2004, **271**, 119-128.

20. H. Deng, G. Fan and Y. Wang, *Synth. React. Inorg. Met.-Org. Chem.*, 2014, **44**, 1306-1311.

21. L. Calvo, M. A. Gilarranz, J. A. Casas, A. F. Mohedano and J. J. Rodriguez, *Ind. Eng. Chem. Res.*, 2005, **44**, 6661-6667.

22. L. Calvo, M. A. Gilarranz, J. A. Casas, A. F. Mohedano and J. J. Rodriguez, *Appl. Catal. B: Environ.*, 2008, **78**, 259-266.

23. M. A. Lillo-Ródenas, J. Juan-Juan, D. Cazorla-Amorós and A. Linares-Solano, *Carbon*, 2004, **42**, 1371-1375.

24. G. Yuan and M. A. Keane, *Appl. Catal. B: Environ.*, 2004, **52**, 301-314.

25. E. Diaz, J. A. Casas, A. F. Mohedano, L. Calvo, M. A. Gilarranz and J. J. Rodriguez, *Ind. Eng. Chem. Res.*, 2008, **47**, 3840-3846.

26. J. Halasz, S. Meszaros and I. Hannus, *React. Kinet. Catal. Lett.*, 2006, **87**, 359-365.

27. G. Yuan and M. A. Keane, *Catal. Commun.*, 2003, **4**, 195-201.

28. I. Witońska, A. Królak and S. Karski, *J. Mol. Catal. A: Chem.*, 2010, **331**, 21-28.

29. S. Karski, *J. Mol. Catal. A: Chem.*, 2006, **253**, 147-154.

30. S. Karski, I. Witońska and J. Gołuchowska, *J. Mol. Catal. A: Chem.*, 2006, **245**, 225-230.

31. I. A. Witońska, M. J. Walock, M. Binczarski, M. Lesiak, A. V. Stanishevsky and S. Karski, *J. Mol. Catal. A: Chem.*, 2014, **393**, 248-256.

32. Z. Dong, X. Le, C. Dong, W. Zhang, X. Li and J. Ma, *Appl. Catal. B: Environ.*, 2015, **162**, 372-380.

33. J. A. Baeza, L. Calvo, M. A. Gilarranz, A. F. Mohedano, J. A. Casas and J. J. Rodriguez, *J. Catal.*, 2012, **293**, 85-93.

34. M. A. Aramendia, V. Borau, I. M. Garcia, C. Jimenez, F. Lafont, A. Marinas, J. M. Marinas and F. J. Urbano, *J. Catal.*, 1999, **187**, 392-399.

35. M. A. Keane, *J. Chem. Technol. Biotechnol.*, 2005, **80**, 1211-1222.

36. G. S. Pozan and I. Boz, *J. Hazard. Mater.*, 2006, **136**, 917-921.

37. G. Yuan and M. A. Keane, *Chem. Eng. Sci.*, 2003, **58**, 257-267.

38. G. Yuan and M. A. Keane, *Catal. Today*, 2003, **88**, 27-36.

39. R. F. Howe, *Appl. Catal. A: Gen.*, 2004, **271**, 3-11.

40. A. Santos, P. Yustos, A. Quintanilla, S. Rodriguez and F. Garcia-Ochoa, *Appl. Catal. B: Environ.*, 2002, **39**, 97-113.

41. J. Sun, G. Yu, L. Liu, Z. Li, Q. Kan, Q. Huob and J. Guan, *Catalysis Science & Technology*, 2014, **4**, 1246-1252.

42. Y. Deng, D. Qi, C. Deng, X. Zhang and D. Zhao, *J. Am. Chem. Soc.*, 2008, **130**, 28-29.

43. X. Le, Z. Dong, Y. Liu, Z. Jin, T.-D. Huy, M. Le and J. Ma, *J. Mater. Chem. A*, 2014, **2**, 19696-19706.

44. M. Xie, F. Zhang, Y. Long and J. Ma, *RSC Advances*, 2013, **3**, 10329-10334.

45. M. Zhu and G. Diao, *The Journal of Physical Chemistry C*, 2011, **115**, 24743-24749.

46. L. Bing, *Sens. Actuators, B*, 2014, **198**, 342-349.

47. Y. Liu, X. Li, X. Le, W. Zhang, H. Gu, R. Xue and J. Ma, *New J. Chem.*, 2015, **39**, 4519-4525.

48. Y. S. Liu, Z. P. Dong, X. L. Li, X. D. Le, W. Zhang and J. T. Ma, *Rsc Advances*, 2015, **5**, 20716-20723.

49. X. Le, Z. Dong, X. Li, W. Zhang, M. Le and J. Ma, *Catal. Commun.*, 2015, **59**, 21-25.

50. Y. Wang, B. Li, L. Zhang, P. Li, L. Wang and J. Zhang, *Langmuir : the ACS journal of surfaces and colloids*, 2012, **28**, 1657-1662.

51. D. P. Wang and H. C. Zeng, *Chem. Mater.*, 2011, **23**, 4886-4899.

52. L. A. Rocha, J. M. Caiut, Y. Messaddeq, S. J. Ribeiro, M. A. Martines, C. Freiria Jdo, J. Dexpert-Ghys and M. Verelst, *Nanotechnology*, 2010, **21**, 155603.

53. H. Chen, S. Liu, H. Yang, Y. Mao, C. Deng, X. Zhang and P. Yang, *Proteomics*, 2010, **10**, 930-939.

54. D. Shen, J. Yang, X. Li, L. Zhou, R. Zhang, W. Li, L. Chen, R. Wang, F. Zhang and D. Zhao, *Nano Lett.*, 2014, **14**, 923-932.

55. Y. Han, D. Zhang, L. L. Chng, J. Sun, L. Zhao, X. Zou and J. Y. Ying, *Nat Chem*, 2009, **1**, 123-127.

56. Q. Huo, D. I. Margolese and G. D. Stucky, *Chem. Mater.*, 1996, **8**, 1147-1160.

57. W. Zhao, J. Gu, L. Zhang, H. Chen and J. Shi, *J. Am. Chem. Soc.*, 2005, **127**, 8916-8917.

58. W. Hu, B. Liu, Q. Wang, Y. Liu, Y. Liu, P. Jing, S. Yu, L. Liu and J. Zhang, *Chem. Commun.*, 2013, **49**, 7596-7598.

59. H. Gu, J. Wang, Y. Ji, Z. Wang, W. Chen and G. Xue, *Journal of Materials Chemistry A*, 2013, **1**, 12471-12477.

60. E. Diaz, J. A. Casas, A. F. Mohedano, L. Calvo, M. A. Gilarranz and J. J. Rodriguez, *Ind. Eng. Chem. Res.*, 2009, **48**, 3351-3358.

61. C. B. Molina, A. H. Pizarro, J. A. Casas and J. J. Rodriguez, *Appl. Catal. B: Environ.*, 2014, **148**, 330-338.

62. X. Le, Z. Dong, W. Zhang, X. Li and J. Ma, *J. Mol. Catal. A: Chem.*, 2014, **395**, 58-65.

63. G. Yuan and M. A. Keane, *Ind. Eng. Chem. Res.*, 2007, **46**, 705-715.